 doi:10.20944/preprints201710.0182.v1

Article

Effect of LCF Pre-Damage on Very High Cycle Fatigue Behavior of TC21 Titanium Alloy

Nie Baohua [1], Zhao Zihua [2,*], Ouyang Yongzhong [3], Chen Dongchu [1], Chen Hong [1], Sun Haibo [1] and Liu Shu [1]

[1] School of Materials Science and Energy Engineering, Foshan University, Foshan 528000, China; niebaohua121@163.com (N.B.); cdcever@163.com (C.D.); chenhongcs@126.com (C.H.); sunmyseven@126.com (S.H); liushu814194678@126.com (L.S.)
[2] School of Materials Science and Engineering, Beihang University, Beijing, 100191, China
[3] School of Environmental and Chemical Engineering, Foshan University, Foshan 528000, China; ouyang7492@163.com
* Correspondence: zhzh@buaa.edu.cn; Tel.: +86-010-8231-3264

Abstract: The effect of low cycle fatigue (LCF) pre-damage on the subsequent very high cycle fatigue (VHCF) behavior is investigated in TC21 titanium alloy. LCF pre-damage is applied under 1.8% strain amplitude up to various fractions of the expected life and subsequent VHCF properties are determined using ultrasonic fatigue tests. Results show that 5% of LCF pre-damage insignificantly affects the VHCF limit due to the absent of pre-crack, but decreases the subsequent fatigue crack initiation life estimated by Pairs' law. Pre-cracks introduced by 10% and 20% of LCF pre-damage significantly reduce the subsequent VHCF limits. The crack initiation site shifts from subsurface-induced fracture for undamaged and 5% of LCF pre-damage specimens to surface pre-crack for 10% and 20% of LCF pre-damage specimens in very high cycle region. The fracture mechanism analysis indicate that LCF pre-crack will re-start to propagate under subsequently low stress amplitude when stress intensity factor of pre-crack is larger than its threshold. Furthermore, the predicted fatigue limits based on EI Haddad model for the LCF pre-damage specimens well agree with the experimental results.

Keywords: very high cycle fatigue; fatigue pre-damage; titanium alloy; LCF

1. Introduction

Titanium alloy is widely used for aeronautical structures because of its high specific strength, toughness, and damage tolerance [1]. Throughout the ultra-long time service, the components are subjected to high frequency, low amplitude, and cyclic load, thus very high cycle fatigue of titanium alloys in the life regime beyond 107 cycles has been drawing a world wide attention. In practice, aeronautical structures may consist of low cycles fatigue (LCF) resulting from the take off and drop down of the aircraft and VHCF generated by high-frequency vibrations. VHCF cracks mainly induced from the metallurgical defects such as non-metallic inclusions [2,3], while LCF crack initiated from the specimen surface due to the surface machining flaws and persist slip bands. Thus interest is increasing not only in the capability of pure VHCF but also in that of VHCF combined with LCF fatigue damage.

Most recent studies have focused on very high cycle fatigue of titanium alloys under constant amplitude. The S–N curves exhibit either a decreasing shape [3, 4] or a step-wise[4]. These materials also exhibit shifting crack initiation site from surface-induced fracture at low cycle regimes to subsurface-induced fracture at very high cycle regimes [5,6]. Microstructure features such as primary α phase size and distribution [7], crystal orientation [8,9], as well as super grain (grain clusters with similar orientation)[10], and stress ratio[11], loading models[12] are important factors affecting the fatigue crack initiation of titanium alloy. However, few studies have been devoted to the LCF/VHCF combined fatigue behavior of titanium alloys. Hang[13] developed continuum damage mechanics model to evaluate cumulative damage of LCF and VHCF for low carbon-manganese steel, indicating that LCF load significantly influences the VHCF strength.

Preprints (www.preprints.org) | NOT PEER-REVIEWED | Posted: 30 October 2017 doi:10.20944/preprints201710.0182.v1

Mayer[14] showed that the deleterious influence of low load cycles below constant amplitude fatigue limit is underestimated for very high cycle fatigue damage of 100Cr6 steel under variable amplitude (VA) loading condition. Treating VHCF as pure failure modes in fatigue design practice is non-conservative throughout ultra-long life service. Furthermore, the effect of LCF load on VHCF fracture mechanism for titanium alloys is not well understood.

The effect of LCF pre-damage on VHCF behavior of TC21 titanium alloy was investigated in the present work. The LCF up to various fractions of expect life was used to introduce pre-damage, and then the VHCF behaviors were subsequently characterized. This work aimed to enable fundamental understanding of very high cycle fatigue fracture mechanism combined with LCF pre-damage.

2. Experimental procedures

2.1. Materials

The material used in this study was TC21 titanium alloy with a nominal chemical composition of Ti-6Al-2Sn-2Zr-3Mo-1Cr-2Nb. Heat treatment was as follows: 900 °C for 2 h + air quenching, and then 600 °C for 4 h + air quenching. The heat-treated material had a high yield strength of 970 MPa and tensile strength of 1070 MPa. A double lamellar basket-weave microstructure was observed (Fig. 1).

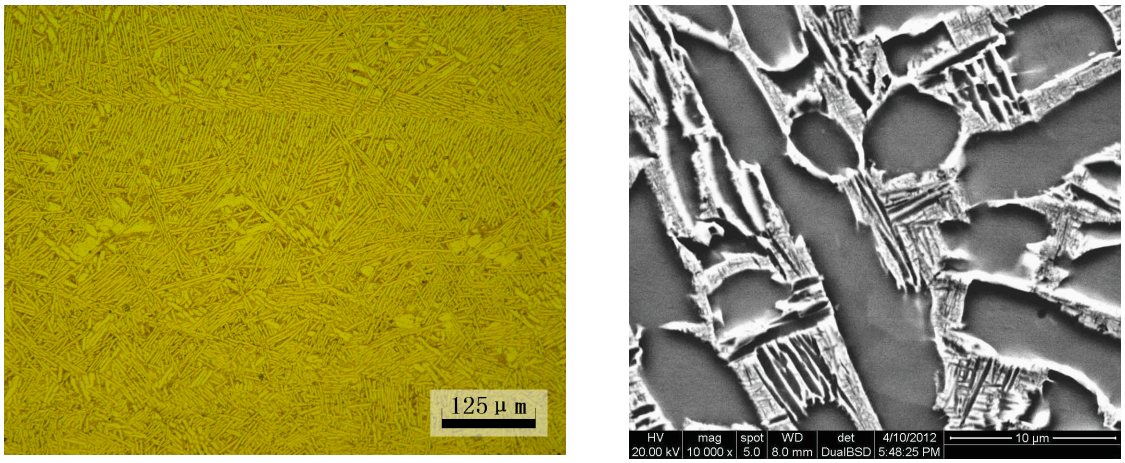

(**a**) (**b**)

Figure 1. Basketweave microstructures of TC21 titanium alloy: (**a**) optical micrograph and (**b**) backscattered electron micrograph.

2.2 Surface treatment

The specimens underwent electro-polishing (EP) to remove the machining layers to observe fatigue damage morphology and eliminate its influence on fatigue behavior. Electro-polishing was carried out in 59% methanol, 35% n-butanol, 6% perchloric acid under -20℃temperature and 20-25V voltage.

2.3 Fatigue test

2.3.1 Ultrasonic fatigue test

Fatigue tests were carried out using an ultrasonic fatigue test machine (20 kHz) at a constant load ratio of R = -1. The ultrasonic fatigue testing method is an accelerated testing method with a frequency far beyond that of conventional fatigue experiments, which brings advantages of effectiveness and economy characters for very high cycle fatigue tests comparing with conventional tests method. The some basic components of an ultrasonic fatigue test machine are shown in Fig. 2 [15]. An ultrasonic generator transforms 50 or 60 Hz voltage signal into sinusoidal signal with 20 kHz; a piezoelectric converter excited by the generator transforms the electrical signal into longitudinal mechanical vibration with same frequency; an ultrasonic horn amplifies the vibration

Preprints (www.preprints.org) | NOT PEER-REVIEWED | Posted: 30 October 2017 doi:10.20944/preprints201710.0182.v1

displacement in order to obtain the required strain amplitude in the middle section of specimen; a computer control system is necessary to control the load amplitude and acquire test data. The maximum displacement amplitude measured by means of a dynamic sensor is obtained at the end of the specimen, while the strain excitation in push-pull cycles (load ratio R=-1) reaches the maximum in the middle section of the specimen, which produces the required high frequency fatigue stress. In addition, compressed air cooling gun is necessary to be used to prevent the temperature increasing of specimen in the tests.

Considering that the amplifier and the specimen must work at resonance, the specimen geometry was designed using the elastic wave theory. Fig. 3 shows the geometries of the fatigue specimens and its dimensions.

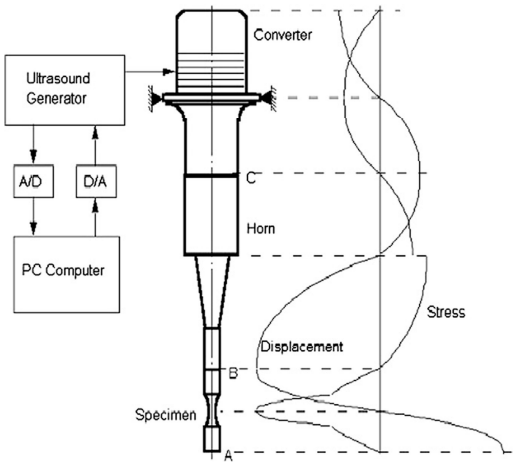

Figure 2. The schematic diagram of ultrasonic fatigue test system [15].

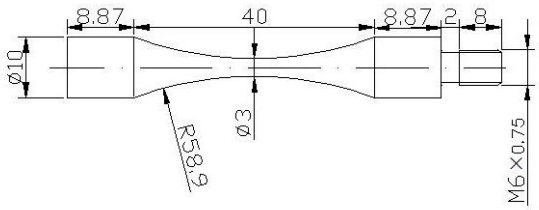

Figure 3. Shape and dimensions of the test specimens.

2.3.2 LCF fatigue tests

The specimen were tested under uniaxial constant strain amplitude controlled strain ratio was then approximately R=1. The Instron 8801 fatigue machine is employed to perform the LCF tests.

Considering the dimensions of ultrasonic fatigue test specimens (Fig.3), LCF test was controlled under transverse diameter deformation. The diameter deformation can be converted to longitudinal direction through the formulas below [13]:

$$\varepsilon_p = -\frac{1}{\nu_p}(\varepsilon_{dia} + \nu_e \frac{\sigma}{E}) \quad (1)$$

$$\varepsilon = \frac{\sigma}{E}(1 - \frac{\nu_e}{\nu_p}) - \frac{1}{\nu_p}\varepsilon_{dia} \quad (2)$$

where ε_{dia}, ε_p, ε are diameter deformation, longitudinal plastic strain, longitudinal total strain, respectively. E, υ_e are Young modulus, elastic Poisson coefficient. υ_p is plastic Poisson coefficient and its value is always 0.5. σ is the longitudinal stress.

In all LCF tests, reversed triangle strain waveform was submitted to the specimens. The failure condition is set as its maximum stress decreasing 20% after its cyclic saturation. Fig. 4 shows fatigue life is 1864 cycles at 1.8% strain amplitude. Furthermore, the fatigue damage morphology of different stage fatigue were observed using a video microscope .

Preprints (www.preprints.org) | NOT PEER-REVIEWED | Posted: 30 October 2017 doi:10.20944/preprints201710.0182.v1

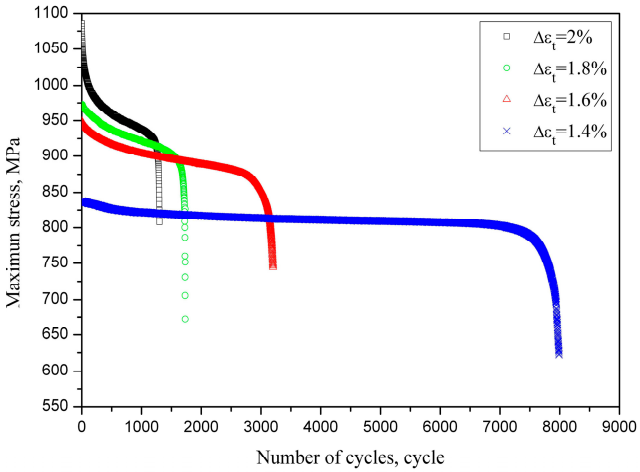

Figure 4. Cycle strain-stress response and fatigue life of TC21 titanium alloy

2.3.3. LCF/VHCF combined fatigue tests

In order to investigate the effect of LCF pre-damage on behavior of VHCF for TC21 titanium alloy, specimens were submitted to a same prior 1.8% strain range (strain ratio: -1). LCF pre-damage was applied onto ultrasonic fatigue specimens at 1.8% strain range for 90 cycles (5% of fatigue life), 180cycles (10% of fatigue life), 360 cycles (20% of fatigue life), respectively. The subsequent VHCF tests are performed by using ultrasonic fatigue test machine at R = -1, room temperature.

2.3.4 Fatigue pre-crack propagation

Fatigue pre-crack was obtained by LCF at 1.8% strain range and ratio of -1. The propagation of fatigue pre-crack under subsequently low stress amplitude were observed using a video microscope. Fatigue crack propagation rate was expressed as follows:

$$da / dN = \frac{\Delta a}{\Delta N} = \frac{a_{i+1} - a_i}{N_{i+1} - N_i} \quad (3)$$

where a_i is crack depth at cycle number N_i, which is supposed to be equal to 0.8c [16], and a surface crack with length 2c was obtained using the video microscope.

3. Results

3.1 LCF damage of TC21 titanium alloy

The LCF surface damage evolution of TC21 titanium alloy under 1.8% strain amplitude is shown in Fig.5. No surface crack is observed in 90 cycles (5% of LCF life) until the number of cycles increase to 180 cycles (about 10% of LCF life). However, the number of microcrack significantly increase in 360 cycles (about 20% of LCF life), then these microcrack were expanded to merge until the specimen is broken.

Preprints (www.preprints.org) | NOT PEER-REVIEWED | Posted: 30 October 2017 doi:10.20944/preprints201710.0182.v1

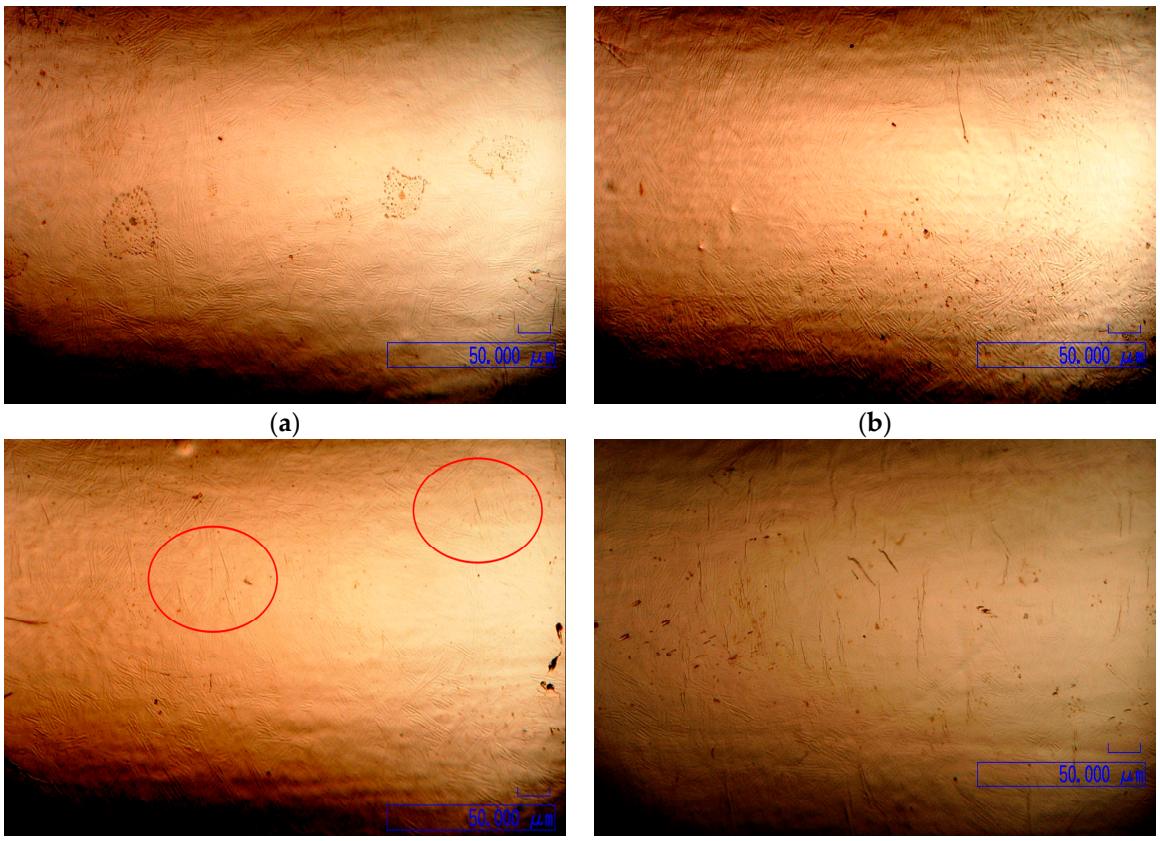

(**a**) (**b**)

(**c**) (**d**)

Figure 5. LCF surface damage evolution of TC21 titanium alloy under 1.8% strain range: (**a**) N=0 cycles ; (**b**) N=90cycles (5%); (**c**) N=180 cycles (10%); (**d**) N=360 cycles (20%).

The fracture surfaces of specimens under 1.8% strain range, Nf = 1864 cycles are shown in Fig. 6. LCF cracks initiate from multiple sites on the sample surface, and a radial ridge pattern parallel to the crack propagation direction is observed on the fracture surface (Fig. 6a). Some small elliptical planes have traces of friction at the fatigue crack initiation site (Figs. 6b and 6c), indicating these small cracks were expanded to merge to fracture, as is accordance with Fig.5d. Cleavage character is observed near the small planes (Fig. 6c). And typical fatigue striation is displayed on fatigue crack steady propagation(Fig. 6d).

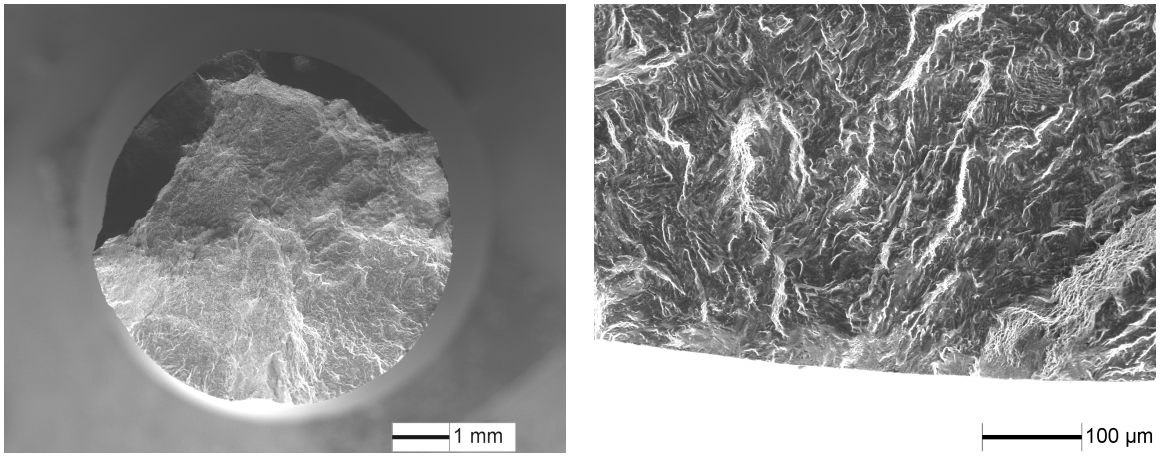

(**a**) (**b**)

Preprints (www.preprints.org) | NOT PEER-REVIEWED | Posted: 30 October 2017 doi:10.20944/preprints201710.0182.v1

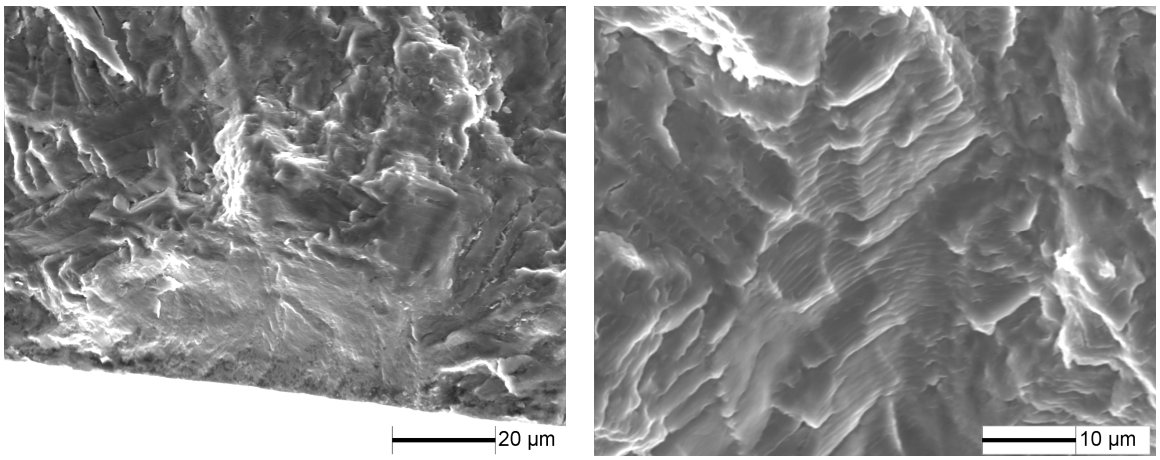

(**c**) (**d**)

Figure 6. Fatigue fracture surface of TC21 alloy under 1.8% strain range, N = 1864 cycles: (**a**) macroscopic morphology, (**b**) crack initiation morphology, (**c**) crack initiation character, and (**d**) crack propagation morphology.

3.2 S-N curves after fatigue pre-damage

Fig.7 shows that the S–N curve of undamaged specimens exhibit either a step-wise, which is similar to the reference [4,5], while the pre-damaged specimens exist knee of horizontal lines for their S-N curves when fatiue life is higher than 105 cycles. 5% of LCF pre-damage insignificantly affects fatigue limit but remarkably decreases fatigue life above fatigue limit compared with undamaged specimens. Fatigue life at 500 MPa stress amplitude is reduced by two orders of magnitude after 5% of LCF pre-damage. Fatigue limits for 10% and 20% of the expected life pre-damage decrease from 430 MPa to 350 MPa and 250 MPa for the undamaged specimens, respectively. However, it was reported that the LCF pre-damage with high R value insignificantly affects fatigue limit because of its overloading effect [17,18]. In this paper, residual compressive stress is introduced at the pre-crack tip because of tensile overload; however, the pre-crack that acts as a blunt notch yields a residual tensile stress due to the high compression overload for a stress ratio of -1. Thus, the overloading effect of the alloy is significantly reduced by the residual tensile stress.

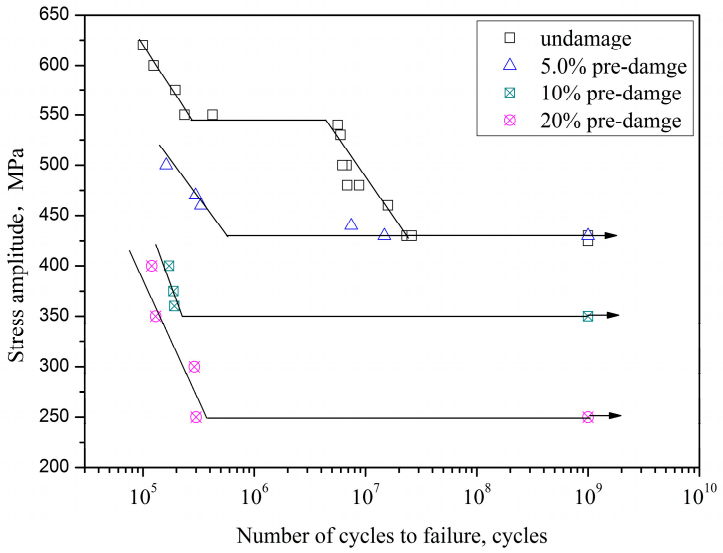

Figure 7. S-N curves of TC21 for LCF pre-damage specimens

3.3 Fracture character of fatigue pre-damage specimens

As is showed in Fig.8, fatigue crack of TC21 titanium alloy under low stress amplitude initiates from the subsurface. α/β lamellar characteristics are observed at the crack initiation site where fine

Preprints (www.preprints.org) | NOT PEER-REVIEWED | Posted: 30 October 2017 doi:10.20944/preprints201710.0182.v1

granular area (FGA) is found along the α lamellar. The FGA characteristics of TC21 titanium alloy are similar to those of high-strength steels [19,20], although non-metallic inclusions are not observed at the FGA center.

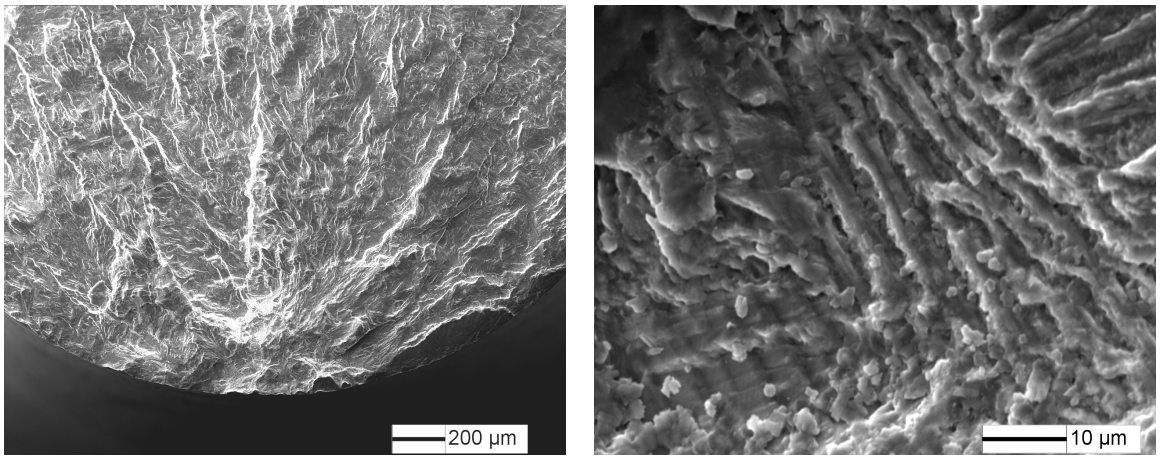

(**a**) (**b**)

Figure 8. Fatigue fracture surface of TC21 titanium alloy at σ = 480 MPa and N = 6.86 × 10^6 cycles: (**a**) fatigue crack initiation site, and (b) high magnification morphology of crack initiation site.

The typical fatigue fracture surfaces of 5% of LCF pre-damage specimens are shown in Figs. 9 and 10. fatigue crack initiates from the specimen surface at 470 MPa stress amplitude (Fig. 9), while fatigue crack tends to initiate from the specimen subsurface for undamaged specimen (Fig. 8). Radial ridge pattern parallel to the crack propagation direction is displayed on the fracture surface. However, fatigue crack initiates from the specimen subsurface at VHCF limit stress amplitude (430MPa), and a fine granular area is observed at the crack initiation site (Fig. 10), which has similar crack initiation character to undamaged specimens.

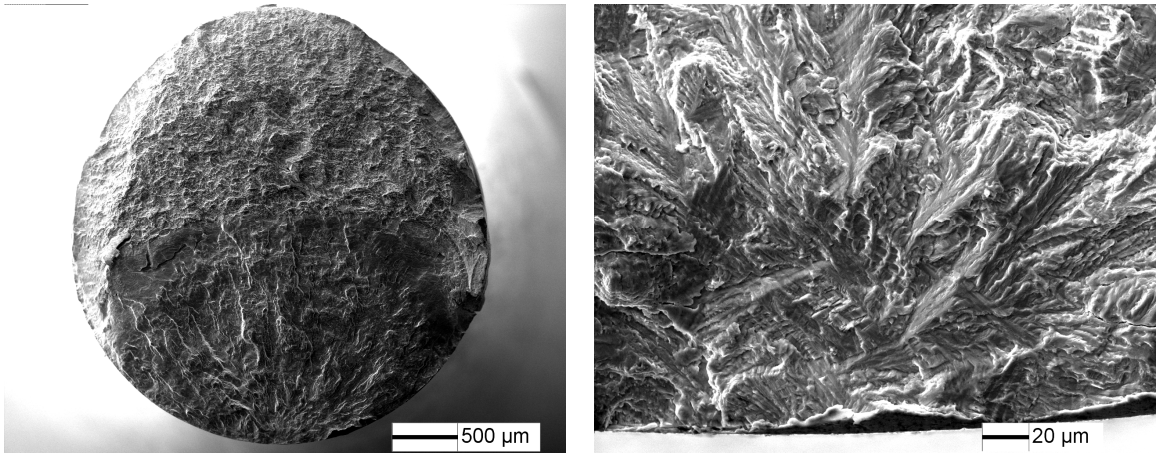

(**a**) (**b**)

Figure 9. Fracture surface for 5% of LCF pre-damage specimens at σ = 470 MPa and N = 1.27 × 10^5 cycles: (**a**) macroscopic morphology, and (**b**) crack initiation character.

Preprints (www.preprints.org) | NOT PEER-REVIEWED | Posted: 30 October 2017 doi:10.20944/preprints201710.0182.v1

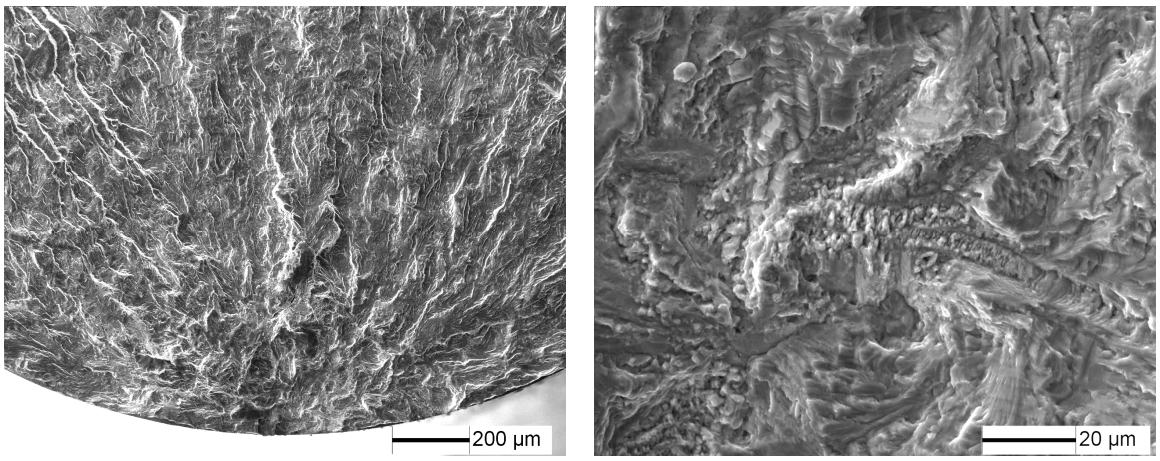

(**a**) (**b**)

Figure 10. Fracture surface for 5% of LCF pre-damage specimens at σ = 430 MPa and N = 1.48 × 10^7 cycles: (**a**) macroscopic morphology, and (**b**) crack initiation character.

Fatigue fracture surfaces of 10% and 20% of LCF pre-damage specimens at low stress amplitude are shown in Figs. 11 and 12. Fatigue crack initiates from the specimen surface (Figs. 11a,12a), and a small elliptical plane with traces of friction is observed at the fatigue crack initiation site (Figs. 11b,12b), similar to that of LCF crack. And the depth of the small plane is approximately 14.7 μm and 41.5 μm, respectively. Moreover, crack-propagation morphology is observed outside the small plane at the crack initiation site. The crack-propagation character is associated with α/β lamellar microstructure generated by the subsequent low stress fatigue, rather than the cleavage morphology generated by LCF. Therefore, the small plane at crack initiation site is supposed to be formed from fatigue pre-cracks.

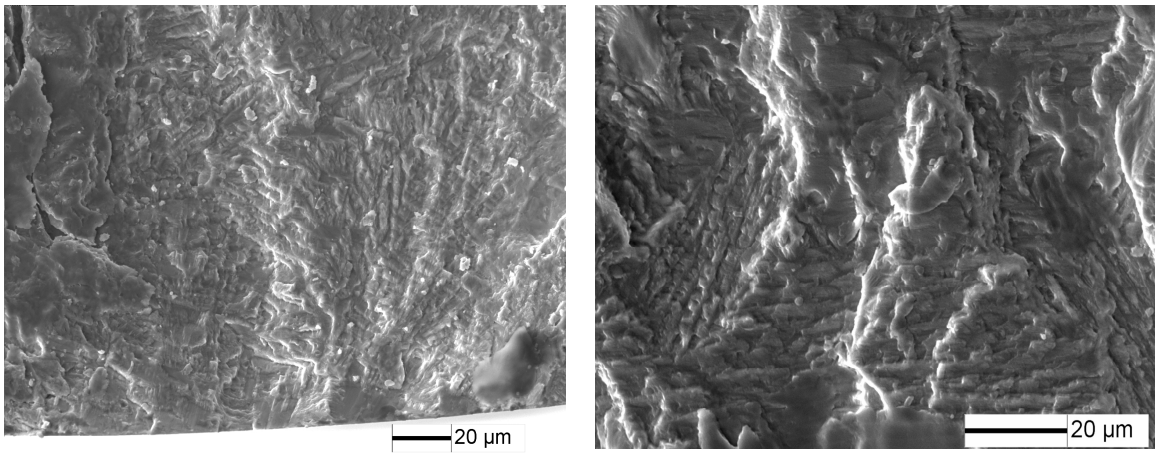

(**a**) (**b**)

Figure 11. Fracture surface for 10% of LCF pre-damage specimens atσ= 375 MPa and N = 1.88 × 10^5 cycles: (**a**) crack initiation character, and (**b**) crack propagation character

Preprints (www.preprints.org) | NOT PEER-REVIEWED | Posted: 30 October 2017 doi:10.20944/preprints201710.0182.v1

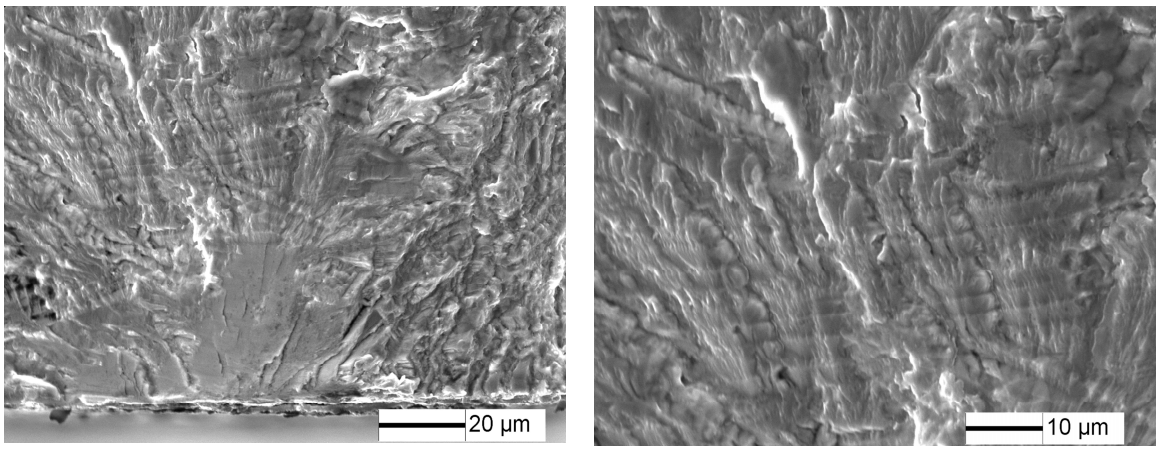

(**a**) (**b**)

Figure 12. Fracture surface for 20% of LCF pre-damage specimens at σ = 350 MPa and N = 1.35 × 10^5 cycles: (**a**) crack initiation character, and (**b**) crack propagation character.

4. Discussions

4.1 Effect of LCF pre-damge on VHCF fracture mechanism

For 5% of LCF pre-damage, the fatigue pre-crack is not formed by the fatigue pre-damage, however, it reduces the resistance of crack initiation by activating the slip systems. According to weaken chain theory, fatigue pre-damage is a weak point, and then fatigue cracks can initiate from the activating slip systems at high stress amplitude [21], as is shown in Fig. 9a, and 5% of LCF pre-damge decreases fatigue properties of TC21 titanium alloy. However, the activating slip systems do not result in the surface fatigue crack initiation at VHCF limit, while fatigue crack initiates from the specimen subsurface at VHCF limit. The results indicates that fatigue early damage occurred at sample surface rather than sample interior.

The pre-crack with the approximately 14.7 μm and 41.5 μm depth are introduced by 10% and 20% fatigue damage. According to EI Haddad fatigue small crack theory, the pre-crack is considered as small cracks, and the stress intensity factor ΔK can be expressed as[22]:

$$\Delta K = Y\sigma_a\sqrt{\pi(a+a_0)} \tag{4}$$

Where σ_a is the stress amplitude, Y is the geometry factor for a surface crack expressed as the reference [3]. The size of a small defect a is the length of the pre-crack, and the intrinsic crack length a_0 is given by [23]:

$$a_0 = \frac{1}{\pi}\left(\frac{\Delta K_{th}}{Y\Delta\sigma_{e,n}}\right)^2 \tag{5}$$

Where $\Delta\sigma_{e,n}$ is the stress range at the fatigue limit of an undamaged specimen, ΔK_{th} is the threshold of fatigue crack growth. The value of ΔK_{th} can be estimated usingΔK_{FGA} [24], which is the threshold of the stress intensity factor for FGA (Fig. 8b) and can be calculated by the following formula:

$$\Delta K_{FGA} = 0.5\sigma_a\sqrt{\pi\sqrt{area_{FGA}}} \tag{6}$$

where and $area_{FGA}$ is the area of FGA.

Thus, ΔK_{FGA} is equal to 2.78 MPam1/2 based on Fig.8. The fatigue limit of TC21 alloy is about 430 MPa (Fig. 7), and the intrinsic crack length a_0 is about 27.56 μm, as obtained from Eq. (5). The stress intensity factors of 10% and 20% fatigue pre-cracks under 375MPa and 280MPa stress amplitude slightly above its endure limits (Fig.7) are 3.02 MPam1/2 and 2.86$MPam^{1/2}$, which are higher than ΔK_{th}. It indicated that the pre-cracks will steadily propagate.

The effect of fatigue pre-crack on the fatigue limit of TC21 alloy can be described using the EI Haddad model. The fatigue limit for specimens with a small pre-crack is defined as follows [24]:

Preprints (www.preprints.org) | NOT PEER-REVIEWED | Posted: 30 October 2017 doi:10.20944/preprints201710.0182.v1

$$\Delta\sigma_{e,n} = \frac{1}{\pi}\left(\frac{\Delta K_{th}}{Y(a+a_0)}\right)^2 \quad (7)$$

According to Eq. (7), the fatigue limit of TC21 alloy with 10% and 20% of LCF pre-damage is about 347.3 and 261.6 MPa, respectively, which well agrees with the experimental data (Fig.13). This finding suggests that fatigue pre-crack plays a significant role in the reduction of fatigue strength.

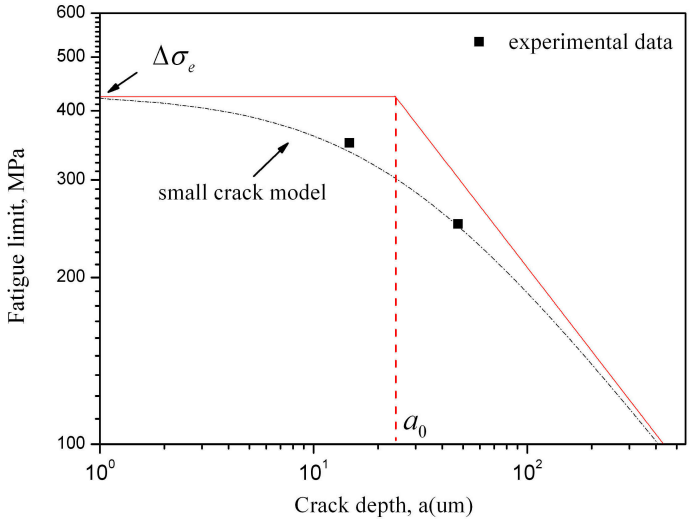

Figure 13. Kitagawa diagram of TC21 titanium alloy with LCF pre-damage

The stress state of the surface initiation crack is regarded as plane stress condition. For mode-I crack, the plastic zone size rc at the crack tip under plane stress condition is [25]:

$$r_c = \frac{1}{\pi}\left(\frac{\Delta K_I}{\sigma_y}\right)^2 \quad (8)$$

Thus the size of the plastic zone for pre-crack is calculated by Eq.(8). For 10% of LCF pre-damage under stress amplitude 375MPa and 20% of LCF pre-damage under stress amplitude 350MPa, the plastic zone is 2.62um and 3.8um, which are much smaller than the size of lamellar basket-weave. This suggest that fatigue early crack growth is significantly influenced by the microstructure (Figs.11b, 12b), which fatigue crack is prone to grow towards the most preferred direction for propagation.

4.2 Effect of fatigue pre-damage on fatigue life

The propagation of the LCF pre-crack follows Paris' law:

$$\frac{da}{dN} = C(\Delta K)^m \quad (9)$$

Fig. 14 shows that the LCF pre-crack propagation rate increases with increased stress intensity factor and can be expressed as:

$$da/dN = 8.64\times10^{-13}(\Delta K)^{5.066} \quad (10)$$

Preprints (www.preprints.org) | NOT PEER-REVIEWED | Posted: 30 October 2017 doi:10.20944/preprints201710.0182.v1

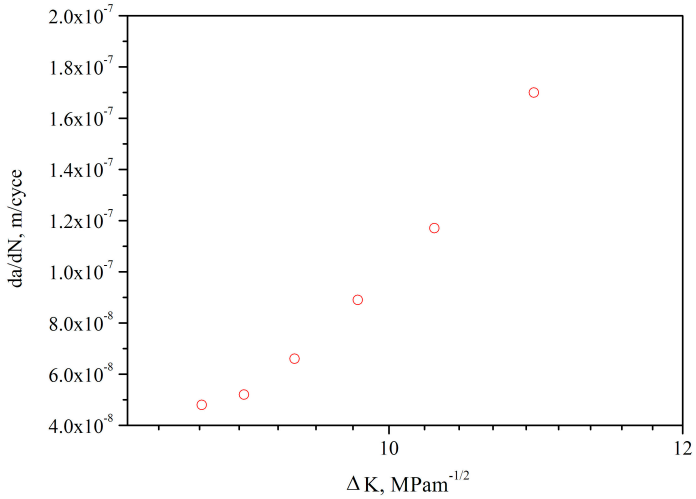

Figure 14. Relation between the expected pre-crack propagation rate da/dN and stress intensity factor ΔK

The LCF pre-crack propagation life under a low stress amplitude can be estimated as:

$$N_{\mathrm{p}} = \frac{(a_{fr}^{1-m/2} - a_0^{1-m/2})}{[1-(m/2)]C(Y\Delta\sigma\sqrt{\pi})^m} \tag{11}$$

where a_{fr} is the size of the fatigue fracture zone. C and m can be obtained by Eq. (10).

The fatigue pre-crack acted as a small crack has a higher propagation rate than that of a long crack with the same nominal stress intensity factor range. An intrinsic crack length a_0 is added to the actual length of crack a to unify the differences in the crack propagation rates between small and long cracks[25]. And the crack propagation rate independent of crack size can be calculated by linear elastic fracture mechanics.

According to Eq. (11), the crack propagation life of TC21 alloy for 5%, 10% and 20% LCF of pre-damage are shown in Table 1. The pre-crack propagation lives for 10% and 20% of LCF pre-damage samples account for a major portion of the expected life, which also indicate that the pre-crack directly propagate under subsequent stress amplitude. However, less than 1% of the expected life is consumed in the crack-propagation life for TC21 alloy without pre-damage. For 5% of LCF pre-damage samples, fatigue pre-crack is not observed at the crack initiation site, but more than 20% of the expected life is consumed in the crack-propagation life, indicating 5% of LCF pre-damage promote the initiation of fatigue crack.

Table 1 Estimation of fatigue crack-propagation life

Pre-damage specimens	Stress amplitude, MPa	N, cycles	a_0, um	a_{fr}, um	Np, cycles	Np/N, %
0%	460	1.590×10^7	27.56	1487	8.008×10^4	0.50
5%	460	3.320×10^5	27.56	1487	8.008×10^4	24.12
10%	350	1.920×10^5	42.26	2427	1.440×10^5	74.99
20%	300	2.000×10^5	69.06	2650	1.706×10^5	85.30

5. Conclusions

The conclusions are summarized as follows:

(1) The S-N curves of pre-damaged specimens exist knee of horizontal lines for 105 ~ 109 cycles. 5% of LCF pre-damage insignificantly affects the VHCF limit due to the absent of pre-crack, but decreases the subsequent fatigue crack initiation life estimated by Pairs' law. Pre-cracks introduced by 10% and 20% of LCF pre-damage significantly reduce the subsequent VHCF limits, which are well predicted based on EI Haddad model.

(2) The crack initiation site shifts from subsurface-induced fracture for undamaged and 5% of LCF pre-damage specimens to surface pre-crack for 10% and 20% of LCF pre-damaged specimens. LCF pre-crack will re-start to propagate under subsequently low stress amplitude when stress intensity factor of pre-crack is larger than its threshold.
(3) 10% and 20% of LCF pre-damage samples account for a major portion of the expected life, while 5% of LCF pre-damage decrease the crack initiation life of fatigue.

Acknowledgments: This work were supported by the National Natural Science Foundation of China (Grant No.51571009, 21405013), Special funds for scientific and technological development of Guangdong (2017A010103029), Scientific and technological program of Foshan (2017AB003941),Construction project of Guangdong province engineering technology research center (506302679076), Construction project of Foshan city scientific research platform (2014AG10009, 2016AG100341), Talent research start-up program of Foshan university(gg040940).

Author Contributions: Zhao Zihua and Chen Hong conceived and designed the experiments; Nie Baohua, Sun Haibo and Liu shu performed the experiments; Chen Dongchu and Ouyang Yongzhong analyzed the data; Nie Baohua wrote the paper.

Conflicts of Interest: The authors declare no conflict of interest.

References

1. Zheng, Y.C.; Zhao, Z.H.; Zhang, Z.H.; Zong, W.M.; Dong, C. Internal crack initiation characteristics and early growth behaviors for very-high-cycle fatigue of a titanium alloy electron beam welded joints. *Mat. Sci. Eng. A* **2017**, *706*, 311-318.
2. Deng, H.; Li, W.; Sakai, T.; Sun, Z. Very high cycle fatigue failure analysis and life prediction of Cr-Ni-W gear steel based on crack initiation and growth behaviors. *Materials* **2015**, *8*, 8338–8354.
3. Nie, B.; Zhang, Z.; Zhao, Z.; Zhong, Q. Very high cycle fatigue behavior of shot-peened 3Cr13 high strength spring steel. *Mater. Design* **2013**, *50*, 503-508.
4. Zuo, J.H.; Wang, Z.G.; Han, E.H. Effect of microstructure on ultra-high cycle fatigue behavior of Ti–6Al–4V Materials. *Mat. Sci. Eng. A* **2008**, *473*, 147-152.
5. Andre, P.; Samuel, F. Effects of inclusions on the very high cycle fatigue behaviour of steels. *Fatigue Fract. Eng. Mater. Struct.* **2017**, *40*, 1694-1707.
6. Stanzl-Tschegg, S. E. Fracture mechanical characterization of the initiation and growth of interior fatigue cracks. *Fatigue Fract. Eng. Mater. Struct.***2017**, *40*, 1741-1751.
7. Crupi, V.; Epasto, G.; Guglielmino, E.; Squillace, A. Influence of microstructure [alpha + beta and beta] on very high cycle fatigue behaviour of Ti-6Al-4V alloy. *Int. J. Fatigue* **2017**, *95*, 64-75.
8. LeBiavant, K.; Pommier, S.; Prioul, C. Local texture and fatigue crack initiaton in a Ti-6Al-4V. *Fatigue Fract. Eng. Mater. Struct.* **2002**, *25*, 527-45.
9. Sinha, V.; Spowart, J.E.; Mills, M.J.; Williams, J.C. Observations on the faceted initiation site in the dwell-fatigue tested ti-6242 alloy: Crystallographic orientation and size effects. *Metall Mater. Trans. A* **2006**, *37*, 1507-18.
10. Ravi Chandran, K.S.; Jha, S.K. Duality of the S–N fatigue curve caused by competing failure modes in a titanium alloy and the role of Poisson defect statistics. *Acta Mater.* **2005**, *53*, 1867-81.
11. Liu, X.; Sun, C.; Hong, Y. Faceted crack initiation characteristics for high-cycle and very-high-cycle fatigue of a titanium alloy under different stress ratios. *Int. J. Fatigue* **2016**, *92*, 434-441.
12. Nikitin, A.; Palin-Luc, T.; Shanyavskiy, A. Crack initiation in VHCF regime on forged titanium alloy under tensile and torsion loading modes. *Int. J. Fatigue* **2016**, *93*, 318-325.
13. Huang, Z.Y.; Wanger, D.; Bathias, C.; Chaboche, J.L. Cumulative fatigue damage in low cycle fatigue and gigacycle fatigue for low carbon-manganese steel. *Int. J. Fatigue* **2011**, *33*, 115-123.
14. Mayer, H.; Haydn, W.; Schuller, R.; Issler, S.; Bacher-Höchst, M. Very high cycle fatigue properties of bainitic high carbon–chromium steel under variable amplitude conditions. *Int. J. Fatigue* **2009**, *31*, 1300-1308.
15. Bathias, C. Piezoelectric fatigue testing machines and devices. *Int. J. Fatigue* **2006**, *28*, 1438–45.
16. Lin, X.B.; Smit, R.A. Finite element modelling of fatigue crack growth of surface cracked plates. Part II: Crack shape change. *Eng. Fract. Mech.***1999**, *63*, 523-540.

17. Morrissey, R.J.; McDowell, D.L.; Nicholas, T. Frequency and stress ratio effects in high cycle fatigue of Ti-6Al-4V. *Int. J. Fatigue* **1999**, *21*: 679-685.
18. Moshier, M.A.; Nicholas, T.; Hillberry, B.M. Load history effects on fatigue crack growth threshold for Ti-6Al-4V and Ti-17 titanium alloys. *Int. J. Fatigue* **2001**, *23*, 253-S258.
19. Hui, W.J.; Zhang, Y.J.; Zhao, X.L.; Hang, D. Very high cycle fatigue properties of Cr-Mo low alloy steel containing V-rich MC type carbides. *Mat. Sci. Eng. A* **2016**, *651*, 311-320.
20. Zhao, P.; Cheng, C.; Gao, G.; Hui, W.; Misra, R.DK.; Bai, B.; Weng, Y. The potential significance of microalloying with niobium in governing very high cycle fatigue behavior of bainite/martensite multiphase steels. *Mat. Sci. Eng. A* **2016**, *650*, 438-444.
21. Lanning, D.; Haritos, G.K.; Nicholas, T.; Maxwell, D.C. Low-cycle fatigue/ high-cycle fatigue interactions in notched Ti-6Al-4V. *Fatigue Fract. Engng. Mater. Struct.* **2001**, *24*, 565-578.
22. Peter, J.O.; Ritchie, R.O. Influence of foreign-object damage on crack initiation and early crack growth during high-cycle fatigue of Ti-6Al-4V. *Eng. Fract. Mech.* **2000**, *67*, 193-207.
23. Liu, Y.; Mahadevan,S. Probabilistic fatigue life prediction using an equivalent initial flaw size distribution. *Int. J. Fatigue* **2009**, *31*, 476–487.
24. Shiozawa, K.; Lu, L. Very high-cycle fatigue behavior of shot-peened high-carbon-chromium bearing steel. *Fatigue Fract. Engng. Mater. Struct.***2002**, *25*, 813-822.
25. Suresh, S. Fatigue of Materials, 2nd ed.; Cambridge University Press: Cambridge, UK, 1998; pp. 388–392.